Available online at www.sciencedirect.com
ScienceDirect
Journal of Catalysis 249 (2007) 123–133
JOURNAL OF CATALYSIS
www.elsevier.com/locate/jcat

# Deactivation and regeneration of iron-containing MFI zeolites in propane oxidative dehydrogenation by $N_2O$

Olga Sánchez-Galofré [a], Yolanda Segura [a], Javier Pérez-Ramírez [a,b,*]

[a] *Institute of Chemical Research of Catalonia (ICIQ), Av. Països Catalans 16, 43007 Tarragona, Spain*
[b] *Catalan Institution for Research and Advanced Studies (ICREA), Pg. Lluís Companys 23, 08010 Barcelona, Spain*

Received 6 January 2007; revised 4 April 2007; accepted 9 April 2007
Available online 1 June 2007

**Abstract**

The $N_2O$-mediated oxidative dehydrogenation of propane over iron-containing MFI zeolites was studied by in situ diffuse reflectance Fourier transform infrared spectroscopy, complemented by analyses in a tapered element oscillating microbalance coupled with gas chromatography and characterization by X-ray diffraction, transmission electron microscopy, and $N_2$ adsorption. Samples with different iron speciation and acidic properties, induced by the preparation method (ion-exchange and steam activation) and the framework composition (Fe–Al–Si, Fe–Ga–Si, and Fe–Ge–Si) were analyzed. Real-time monitoring of the reaction under operando conditions allowed us to gain insight into the mechanism and kinetics of deactivation and coke formation, as well as zeolite regeneration in air. Deactivation of iron zeolites in the oxidative dehydrogenation of propane is caused by coke deposition on active extra-framework iron species. The mechanism of coke formation and the nature of the deposits were similar over the samples, independent of the catalytic performance and deactivation pattern. Regeneration in air led to the disappearance of coke-related bands and the practically complete recovery of the original porosity, while the zeolite crystallinity remained intact. The initial propylene yield over the fresh and regenerated Fe–Ga–Si zeolites was the same, but the latter sample exhibited faster deactivation. This is attributed to a change of iron constitution in the first reaction–regeneration cycle. The alteration of the local environment of the iron species was indirectly concluded from the appearance of a band associated with Lewis centers in the infrared spectra of the regenerated zeolite. In support of this, TEM studies demonstrated an extensive degree of iron clustering as $FeO_x$ nanoparticles in the regenerated catalyst compared with the fresh and coked catalysts.


*Keywords:* Operando spectroscopy; DRIFTS; TEOM; Oxidative dehydrogenation; Iron zeolites; Propane; $N_2O$; Propylene; Deactivation; Coke; Regeneration

## 1. Introduction

Iron-containing pentasyl-type zeolites exhibit unique catalytic properties in $N_2O$-mediated oxidation. The extensive number of studies in this topic was triggered by the accomplishments in the direct hydroxylation of paraffins to alcohols and of aromatic hydrocarbons to phenols [1,2]. More recently, several groups applied these materials in the functionalization of light alkanes for obtaining petrochemicals directly or their respective olefinic feedstocks. Particular emphasis has been put on the $N_2O$-mediated oxidative dehydrogenation of propane (ODHP) to propylene [3–6]. Efficient on-purpose propylene technologies are being required in view of the widening gap between conventional propylene supply and demand [7].

The remarkable ODHP performance of iron zeolites has been related to the specificity of $N_2O$ as a mono-oxygen donor and to the ability of determined iron species for coordinating reactive atomic oxygen species able to efficiently dehydrogenate propane [4]. The most promising zeolitic system reported so far is steam-activated Fe-ZSM-5, displaying initial propene yields up to 25% [4,8]. These results are comparable with the highest values reported over V- and Mo-based catalysts with $O_2$ as the oxidant [9]. A major drawback of iron zeolites in ODHP with $N_2O$ is the deactivation by coke, leading to a rapid decrease of the propylene yield [4]. The tapered element oscillating microbalance (TEOM) technique coupled with gas chromatography (GC) analysis has proved to be a suitable tool for correlating deactivation and mass changes due to coking in the

* Corresponding author. Fax: +34 977 920 224.
*E-mail address:* jperez@iciq.es (J. Pérez-Ramírez).

0021-9517/$ – see front matter 
doi:10.1016/j.jcat.2007.04.010

$C_3H_8 + N_2O$ reaction [10,11]. This information was the basis for the engineering of a cyclic process for continuous propylene production with alternation of reaction, purging, and regeneration steps using a battery of parallel fixed-bed reactors [12,13].

The level of detail and accuracy for in situ investigation of coke formation as obtained by TEOM cannot be accomplished using typical approaches to study deactivation, in which coke is characterized after exposing the catalyst to reaction conditions and taking samples at defined times for ex situ analyses [14–16]. However, TEOM does not provide information on the deactivation mechanism at the catalyst surface level, because the nature of coke as well as its interaction with chemical groups in the zeolite cannot be probed. To gain a better understanding of the deactivation of iron-containing zeolites in the $C_3H_8 + N_2O$ reaction and the subsequent regeneration in air, complementary spectroscopic studies under reaction conditions are needed. In situ FTIR spectroscopy is suitable for assessing coke deactivation of zeolite catalysts in hydrocarbon conversion [17–20], by monitoring in real time the formation of carbonaceous deposits and eventual changes in vibrations associated with the surface acidity and framework of the microporous material.

Observing the evolution of the working catalyst under true process conditions is useful for an improved understanding of the ODHP reaction. To the best of our knowledge, in situ investigations of selective oxidation of hydrocarbons with $N_2O$ over iron-containing zeolites have not been reported. Moreover, the reusability of the regenerated catalysts (i.e., to what extent the catalytic performance is recovered on successive reaction and regeneration cycles) has not yet been addressed in detail. Infrared spectroscopy has been applied to quantitatively characterize the nature and density of Brønsted and Lewis acid centers in the fresh zeolite catalysts by adsorption of probe molecules such as pyridine and $d_3$-acetonitrile over the fresh samples [11,16,21,22]. Based on these infrared characterizations and activity measurements in benzene hydroxylation with $N_2O$, it was concluded that there is no correlation between the acidity and the rate of phenol formation, although the former accelerates the catalyst deactivation by coking.

In the present work, we performed an operando DRIFTS study to gain insight into the kinetics of coke formation and the deactivation mechanism of iron-containing MFI zeolites in the $N_2O$-mediated ODHP, and their subsequent regeneration in air. Infrared results were complemented by TEOM–GC experiments over the catalysts at the same conditions. The degree of catalyst reversibility on reaction and regeneration is evaluated and discussed on the basis of these analyses and characterization of the fresh, coked, and regenerated samples by X-ray diffraction (XRD), transmission electron microscopy (TEM), and nitrogen adsorption.

## 2. Experimental

### 2.1. Catalysts

Table 1 shows the chemical composition of the zeolites investigated in this study. A detailed description of the preparation methods and characterization of the iron speciation and acidity of the samples has been given elsewhere [11,23,24]. Briefly, steam-activated iron zeolites were prepared by hydrothermal synthesis of MFI zeolites with Fe–Ga–Si and Fe–Ge–Si frameworks, followed by calcination at 823 K for 10 h. The nominal molar ratios in the synthesis gels were TPAOH/Si = 0.1, NaOH/Si = 0.2, $H_2O$/Si = 45, Si/Ga = 35, Si/Ge = 250, and Si/Fe = 150. The calcined zeolites were activated in steam (300 mbar $H_2O$ in 30 $cm^3$ STP $N_2$ $min^{-1}$) at 873 K for 5 h; these catalysts are denoted hereinafter as Fe–Ga-st and Fe–Ge-st. The Fe–Al-lie sample was prepared by liquid-ion exchange of commercial $NH_4$-ZSM-5 (P&Q, CBV 8020, nominal Si/Al ratio = 37.5) at room temperature with a diluted aqueous solution of $Fe(NO_3)_3 \cdot 9H_2O$. The ion-exchanged zeolite was washed with deionized water, dried, and calcined in static air at 823 K for 5 h.

Table 1
Chemical composition of the zeolite samples determined by ICP-OES

| Sample | Si (wt%) | Fe (wt%) | Al (wt%) | Ga (wt%) | Ge (wt%) |
|---|---|---|---|---|---|
| Fe–Al-lie | 40.1 | 1.25 | 1.07 | – | – |
| Fe–Ga-st | 42.4 | 0.59 | – | 3.23 | – |
| Fe–Ge-st | 43.4 | 0.67 | – | – | 0.44 |

### 2.2. TEOM–GC

Reaction and coke deactivation studies were carried out in a Rupprecht and Patashnick TEOM 1500 pulse mass analyzer coupled to a gas chromatograph. The experimental procedure and data processing have been described in detail elsewhere [10,11]. Briefly, the TEOM microreactor (4 mm i.d.) was loaded with 30 mg of catalyst particles (sieve fraction 125–250 μm), followed by pretreatment in He at 723 K for 2 h. The ODHP was carried out in a feed mixture of 50 mbar $C_3H_8$ and 50 mbar $N_2O$ in He at ambient pressure and a weight-hourly space velocity (WHSV) of 400,000 ml $h^{-1}$ $g_{cat}^{-1}$. The coke content was determined from the total mass uptake measured by the TEOM, and the product gases were analyzed online by a gas micro-chromatograph (Chrompack CP-2002) equipped with a thermal conductivity detector, using Poraplot Q and Molsieve 5A columns.

### 2.3. Infrared spectroscopy

Fourier transform infrared spectroscopy was carried out in a Nicolet 5700 spectrometer (Thermo Scientific) using a Spectratech collector II diffuse reflectance (DRIFT) accessory equipped with a high-temperature chamber, ZnSe windows, and a MCT detector. The latter was cooled with liquid nitrogen for at least 1 h before the experiments. The equipment was purged with Ar before and during the experiment to prevent traces of humidity in the path of the beam in the spectrometer. The sample cell was filled with ca. 40 mg of powdered catalyst and carefully leveled off with spatula to reduce reflections off the sample surface and to ensure reproducible results. Before the experiments, the sample was pretreated in helium

(100 $cm^3$ STP $min^{-1}$) at the reaction temperature for 20 min, using a ramp rate of 5 K $min^{-1}$. Then the spectrum of the fresh zeolite was obtained using KBr (Aldrich, IR spectroscopy grade) in He at the same temperature as the background. Subsequently, He was replaced by the reaction mixture, and spectra were automatically recorded every 20 s for 120 min. The reaction of propane and nitrous oxide was carried out at 723 K in a mixture of 50 mbar $C_3H_8$ and 50 mbar $N_2O$ in He at ambient pressure, using a total gas flow of 100 $cm^3$ STP $min^{-1}$. Gases were introduced in the cell by means of flow meters, and the outlet flow was recorded continuously during the experiment by a DryCal DC-lite gas-flow calibrator from Biosint. The intensity of the bands related to coke, Brønsted acid centers, and silanol groups in the zeolite during ODHP was monitored at the position of maximum absorbance in each background-corrected spectrum. After the reaction period, the $C_3H_8 + N_2O$ mixture was switched to He (100 $cm^3$ STP $min^{-1}$) for 15 min to flush the cell and to remove weakly adsorbed species on the zeolite surface. Then He was replaced by air, and the regeneration of the catalyst was carried out at 723 K for 90 min. In the reaction and regeneration experiments, the spectra of the reaction mixture and air in KBr, respectively, were taken as references. Spectra were systematically recorded in the range of 650–4000 $cm^{-1}$ by the co-addition of 32 scans and with a nominal resolution of 4 $cm^{-1}$. A fresh sample was normally used in each run. In addition, several reaction–regeneration cycles were conducted over the same sample.

### 2.4. Characterization

The fresh, coked, and regenerated zeolites were characterized by XRD, TEM, and $N_2$ adsorption. Powder XRD patterns were measured in a Siemens D5000 diffractometer with Bragg-Brentano geometry and Ni-filtered Cu$K\alpha$ radiation ($\lambda = 0.1541$ nm). Data were collected in the $2\theta$ range of 5–70° using an angular step of 0.05° and a counting time of 8 s per step. TEM was done using a JEOL JEM-1011 microscope operated at 100 kV and equipped with a SIS Megaview III CCD camera. A few droplets of the sample suspended in ethanol were placed on a carbon-coated copper grid, followed by evaporation at ambient conditions. $N_2$ adsorption–desorption isotherms at 77 K were measured in a Quantachrome Autosorb-1-MP analyzer. Before the measurements, the samples were evacuated at 373 K for 12 h. The BET method [25] was applied to calculate the total surface area, which was used for comparative purposes. The $t$-plot method [26] was used to discriminate between microporosity and mesoporosity.

## 3. Results and discussion

### 3.1. Fresh zeolites

The infrared spectra of the iron-containing zeolites in the CH and OH stretching regions are shown in Fig. 1. The spectra in the framework region (1600–1990 $cm^{-1}$) closely reproduce results in the literature [27] and are not displayed for the sake of conciseness. No bands associated with the template or any sort of organic-related contamination appeared in the region of 2800–3000 $cm^{-1}$. The infrared band at around 3730 $cm^{-1}$ present in the three samples is typically assigned to terminal silanol groups (Si–OH) on the external surface of the zeolite crystal [28]. This absorption also has been attributed to nonacidic silanol groups located in the zeolite pores [29]. The band at 3600 $cm^{-1}$ observed in Fe–Al-lie and Fe–Ga-st corresponds to bridging hydroxyl groups associated with Brønsted acidity [27,28]. This band did not appear in Fe–Ge-st due to the absence of framework Al or Ga.

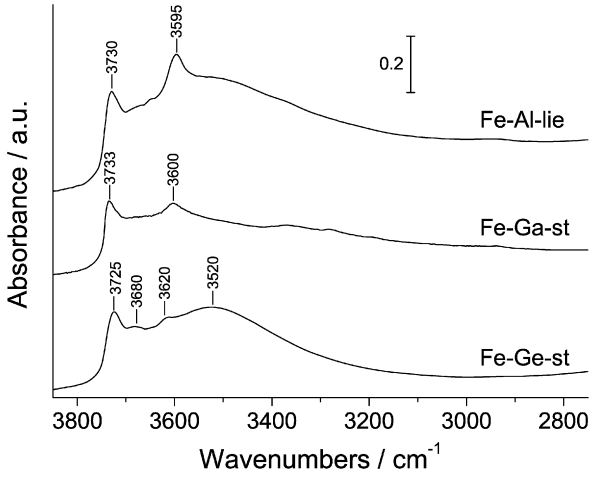


Fig. 1. Infrared spectra of the fresh zeolites in He at 723 K.

The band at 3600 $cm^{-1}$ was considerably more intense in Fe–Al-lie than in Fe–Ga-st, indicating that the former sample was more acidic despite the similar bulk Si/Al and Si/Ga ratios in the samples (ca. 35, Table 1). This certainly was the case, because Fe–Ga-st was activated in steam at high temperature, inducing the hydrolysis of a fraction of Si–OH-Ga groups and resulting in extra-framework gallium species [23]. However, this did not lead to an easily distinguishable absorption at 3650–3700 $cm^{-1}$ in the spectrum of the sample, often related to extra-framework trivalent cations such as $Al^{3+}$ with Lewis acid character [30]. The presence of significant amounts of extra-framework aluminum in Fe–Al-lie also can be excluded attending to the absence of this band.

The Ge-containing zeolite showed weak bands at 3680 and 3620 $cm^{-1}$ and a broad absorption at 3520 $cm^{-1}$. The band at 3680 $cm^{-1}$ is related to the contribution of terminal Ge–OH groups [31,32], which are reported to have an intermediate acidity between bridged hydroxyls and silanol groups. The band at around 3620 $cm^{-1}$ can be assigned to bridging Si(OH)Fe groups [33], which result from the incomplete dislodgement of lattice iron on steaming. It has been demonstrated that the absence of Al and Ga in iron-substituted MFI frameworks induces a less pronounced degree of Fe extraction on steam treatment at a certain condition of temperature and steam partial pressure [23,24,34]. The broad band at 3520 $cm^{-1}$ is typically assigned to hydrogen-bonded silanols resulting from structural defects due to incomplete condensation or removal of lattice atoms [28]. Recent work by van der Water et al. [31] reported that germanium incorporation in the MFI framework caused

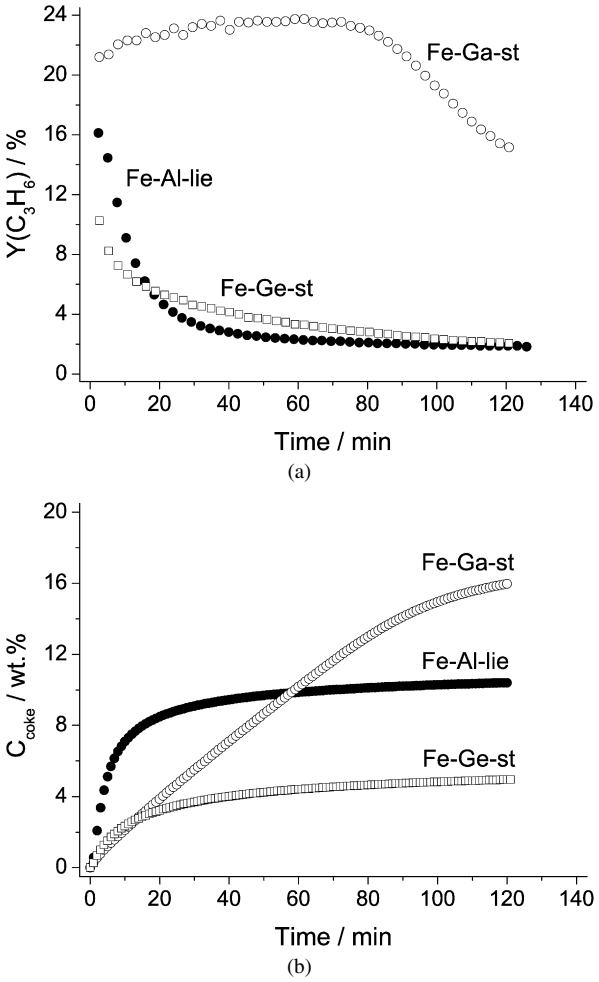


Fig. 2. (a) Propylene yield and (b) coke content vs time over the iron zeolites during ODHP with $N_2O$ at 723 K from TEOM–GC experiments. Conditions are described in Section 2.2.

an increased number of local distortions and defects, originating a greater variety of OH groups. Accordingly, we tentatively assigned this feature to dislocations in the MFI framework connected with germanium substitution. It should be stressed that this feature is not exclusive to Ge-containing zeolites; in fact, the Fe–Al-lie sample exhibited a shoulder at around 3520 $cm^{-1}$ (Fig. 1), indicating defects in this zeolite framework.

### 3.2. ODHP performance

The catalysts considered in this study exhibited distinct ODHP performance. The propylene yield and coke content determined by the TEOM technique coupled to GC analysis is shown in Fig. 2. At 723 K, the initial propylene yield (after 2 min on stream) was higher over Fe–Ga-st (21%) than over Fe–Al-lie (16%) and Fe–Ge-st (10%). As reported elsewhere [8,11], the initial degree of $C_3H_8$ conversion was 45% over Fe–Ga-st, 40% over Fe–Al-lie, and 19% over Fe–Ge-st. The $C_3H_6$ selectivity over the three catalysts ranged from 40 to 50%. The general correlation between the decreased $Y(C_3H_6)$ and the increased amount of coke made it possible to conclude that propylene is the main precursor of coke [10]. The propylene yield decayed rapidly over Fe–Al-lie and Fe–Ge-st, particularly in the liquid ion-exchanged sample (from 16 to 2% during the first 40 min on stream). In contrast, Fe–Ga-st displayed remarkable performance, and the propylene yield was stable for a relatively long period on stream even if large amounts of coke were formed on the sample [$Y(C_3H_6) = 22\%$ and $C_{coke} = 13$ wt% after 80 min]. Apparently, the active iron species in this particular catalyst were not affected (blocked or poisoned) by the carbonaceous deposits. After the 80-min period, the propylene yield decayed progressively, and the rate of coke formation was reduced. Based on TEOM results, the profile of coke buildup over Fe–Al-lie was steeper than over Fe–Ga-st, which can be related to the higher density of Brønsted acid centers in the former sample. Previous studies by some of us have tentatively attributed the outstanding performance of steam-activated MFI zeolites with Fe–Ga–Si and Fe–Al–Si frameworks to a higher number of active iron centers for ODHP and/or to increased resistance toward deactivation by coke deposition [11]. The reduced Brønsted acidity in these samples due to extensive hydrolysis of Si–O–$M^{3+}$ ($M^{3+}$ = Fe, Ga, Al) groups on high-temperature steam treatment and the presence of (limited) mesoporosity also have been identified as possible reasons for the decreased deactivation.

### 3.3. Infrared studies during ODHP

Infrared experiments were conducted at 723 K, which can be considered the optimal temperature for the $N_2O$-mediated propane oxidative dehydrogenation over iron-containing zeolites [11,13]. The evolution of the catalysts in the CH and OH stretching regions during ODHP is shown in Fig. 3. In the experiments, spectra were continuously acquired every 20 s for 120 min, but for clarity, only those at times when representative changes occur are depicted here. Coke-related bands in the region of 2800–3100 $cm^{-1}$ progressively develop during the first 20 min of reaction, with incremental changes thereafter. Coke formation is connected to the presence of strong acidic protons in the zeolite surface, as well as to the presence of trivalent cations ($Fe^{3+}$, $Ga^{3+}$, $Al^{3+}$) as electron acceptor sites [5]. Simultaneous with coke formation, a gradual decrease of the bands at 3600 and 3730 $cm^{-1}$ occurred due to coke deposition on Brønsted acidic centers and terminal silanol groups. It is well known that Brønsted acid sites catalyze the formation of carbenium ions [35,36], where double bonds can oligomerize, initiating the coking process. As shown in Fig. 3, the broad absorption centered at 3520 $cm^{-1}$ in Fe–Ge-st, assigned to hydrogen-bonded silanols connected with framework dislocations, does not experience an apparent change during the ODHP reaction. However, the weak absorption at 3620 $cm^{-1}$ vanishes after 10 min on stream. The latter observation further supports its assignment to Brønsted acidity caused by incomplete extraction of framework iron in the sample on steaming. Characteristic vibrations of the MFI framework did not experience significant changes during the reaction (not shown).

Fig. 4 zooms in the CH stretching region to compare the carbonaceous deposits in the catalysts after 120 min in contact with the $C_3H_8 + N_2O$ mixture at 723 K and switching to he-

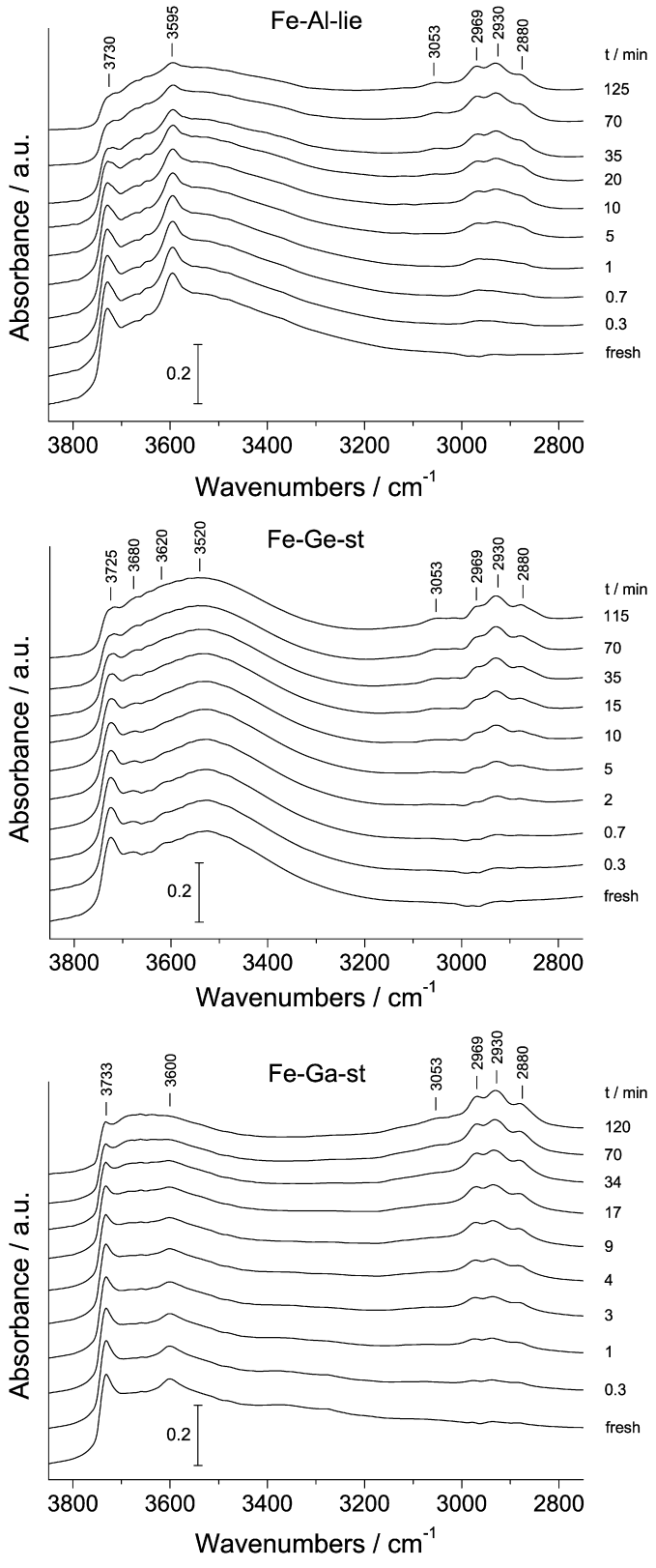


Fig. 3. Infrared spectra of the zeolites at selected times during ODHP with $N_2O$ at 723 K. Conditions are described in Section 2.3.

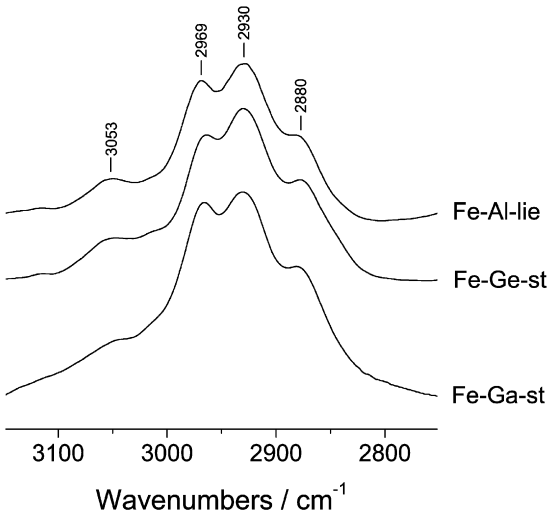


Fig. 4. Infrared spectra in the CH stretching region of the coked catalysts, recorded in He at 723 K after 120 min in $C_3H_8 + N_2O$ at the same temperature.

lium for 15 min at the same temperature. The latter treatment is intended to remove weakly adsorbed species on the samples before infrared analysis. The position and relative intensities of the four absorption bands are very similar, suggesting the similar nature of coke in the samples despite the markedly different catalytic performance. The band at 3053 $cm^{-1}$ is attributed to CH stretching in aromatic groups [37]. The other bands have been assigned to aliphatic compounds; features at 2969 and 2930 $cm^{-1}$ are related to asymmetric CH stretching of $CH_3$ and $CH_2$ groups, respectively, whereas the band at 2880 $cm^{-1}$ is attributed to symmetric CH stretching of $CH_3$ groups [29,37].

The evolution of the band at 2930 $cm^{-1}$ was taken as a measure of the coke build-up during ODHP. As shown in Fig. 5, the intensity of this absorption increased in the first 20 min on stream over the catalysts. After 40–50 min, the intensity did not change over Fe–Al-lie and Fe–Ge-st, but increased over Fe–Ga-st. These results are qualitatively in good agreement with the TEOM profiles in Fig. 2, indicating continuous coke build-up in the latter sample due to its superior ability to produce propylene. Similar trends were obtained when other coke-related bands related to aliphatic groups were considered. This can be anticipated because the intensity ratio of the absorptions at 2880, 2930, and 2969 $cm^{-1}$ did not change significantly along the reaction. Coke was deposited on Brønsted acid centers and terminal silanols in the zeolites, leading to decreases in the bands associated with these groups at 3600 and 3730 $cm^{-1}$, respectively (Fig. 5). The intensity decrease was most pronounced in the more acidic Fe–Al-lie sample, which can be correlated with the faster deactivation of this catalyst (Fig. 2). The relatively fast deactivation of the Fe–Ge-st sample may be due to the limited number of active extra-framework iron sites and the favored coke formation connected with the occurrence of iron in lattice positions. The coke profiles determined by TEOM and in situ DRIFTS agree reasonably well for Fe–Al-lie and Fe–Ge-st. The decrease in propylene yield over these samples was correlated with the increased amount of coke, indicating that deposition of carbonaceous deposits was responsible for catalyst deactivation. In contrast, attending merely to the coke buildup, the higher resistance of Fe–Ga-st toward deactivation (stable $C_3H_6$ production for 80 min) can-

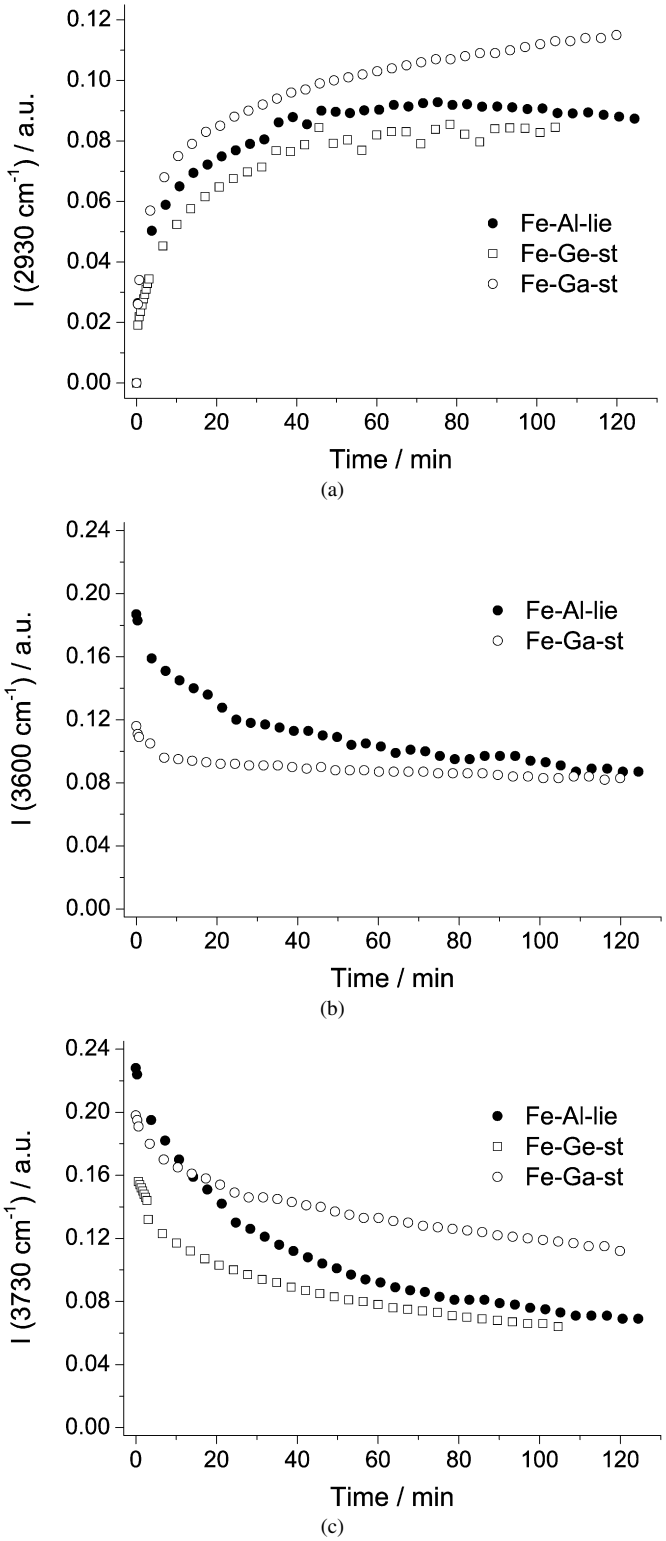


Fig. 5. Intensity of the absorption bands associated with (a) coke (2930 $cm^{-1}$), (b) Brønsted acid centers (3600 $cm^{-1}$), and (c) terminal silanol groups (3730 $cm^{-1}$) over the catalysts during ODHP with $N_2O$ at 723 K.

not be anticipated. This reveals that the coke production was not necessarily accompanied by decreased propylene production. The agreement between the shapes of the coke profiles determined by TEOM and infrared spectroscopy over Fe–Al-lie and Fe–Ge-st is not applicable to Fe–Ga-st. For the latter catalyst, the buildup of carbonaceous deposits determined by DRIFTS appears to be faster than the TEOM-derived profiles. The reason for the mismatch cannot be currently ascertained.

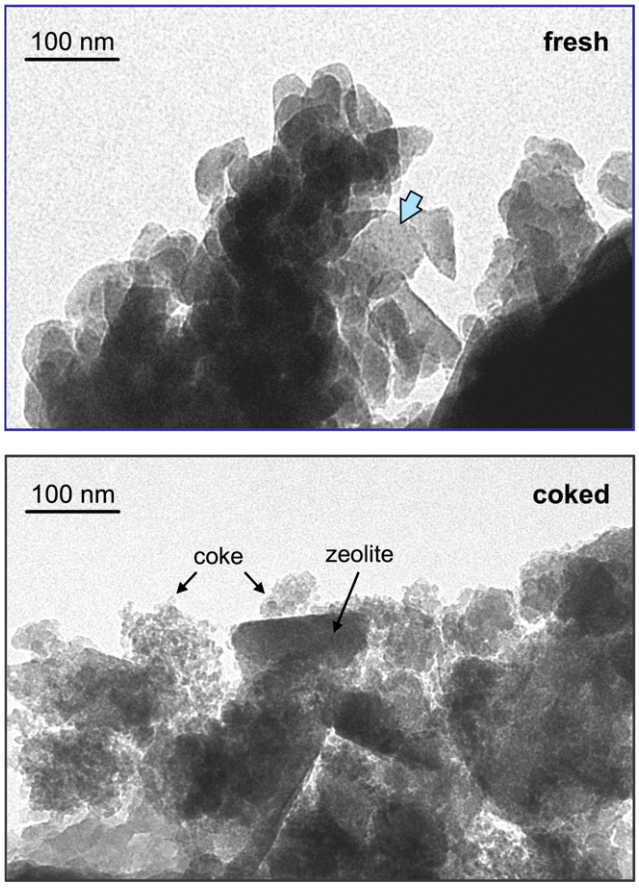


Fig. 6. TEM images of the fresh and coked Fe–Ga-st samples.

### 3.4. Coked zeolites

The color of the zeolites after reaction was black due to the presence of coke, in contrast with the light-yellow (Fe–Ga-st and Fe–Ge-st) or yellow-ocher (Fe–Al-lie) color of the starting zeolites. TEM indicated abundant carbonaceous deposits of amorphous nature coexisting with the zeolite crystals in the sample after use in ODHP at 723 K for 120 min (Fig. 6). In addition, despite its low magnification, iron oxide nanoparticles could be identified in the micrograph of the fresh zeolite (see crystal indicated by the solid arrow). These particles were highly dispersed (size 1–3 nm), as we elaborate on later.

The coked samples were also characterized by $N_2$ adsorption to evaluate the impact of the reaction on the porous characteristics of the zeolite. As shown in Fig. 7, the isotherms of the fresh samples exhibited high nitrogen uptakes at low relative pressures ($p/p_0 < 0.3$), exhibiting the type I behavior typical of microporous materials [38]. The samples exhibited hysteresis at $p/p_0 > 0.45$, which can be attributed to the presence of limited mesoporosity. The porosity parameters resulting from the application of the BET model [25] and the $t$-plot method [26], shown in Table 2, were characteristic of MFI materials. The

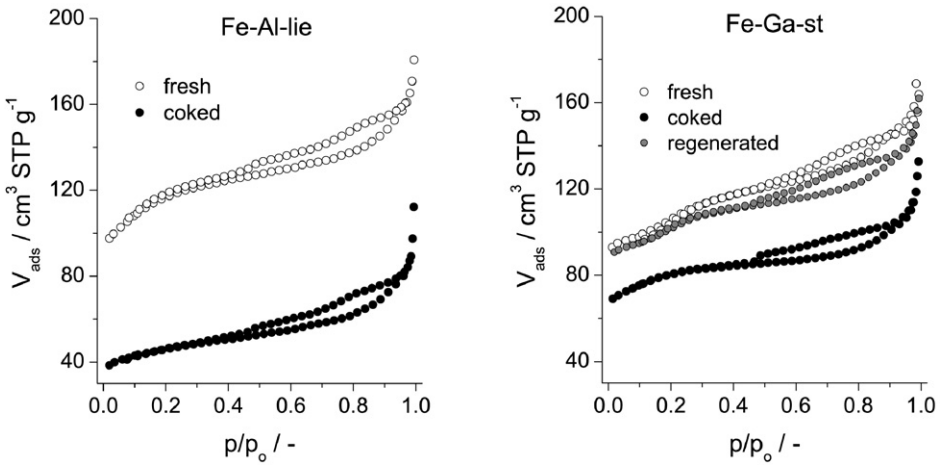


Fig. 7. $N_2$ adsorption–desorption isotherms of selected zeolites.

Table 2
Porous properties of selected zeolites determined by $N_2$ adsorption

| Sample | Form | $V_{pore}$ ($cm^3\ g^{-1}$) | $V_{micro}$ ($cm^3\ g^{-1}$) | $S_{BET}$ ($m^2\ g^{-1}$) | $S_{meso}$ ($m^2\ g^{-1}$) |
|---|---|---|---|---|---|
| Fe–Al-lie | Fresh | 0.26 | 0.17 | 426 | 43 |
| | Coked[a] | 0.15 | 0.06 | 169 | 40 |
| Fe–Ga-st | Fresh | 0.24 | 0.15 | 388 | 51 |
| | Coked[a] | 0.18 | 0.11 | 261 | 31 |
| | Regenerated[b] | 0.23 | 0.14 | 370 | 54 |

[a] After ODHP at 723 K for 120 min.
[b] After regeneration in air at 723 K for 90 min.

$N_2$ uptake of the spent zeolites was significantly reduced due to the presence of coke, but the shape of the isotherms did not change (Fig. 7). The micropore and total pore volumes of Fe–Ga-st were decreased by 25% after ODHP. As expected, the BET surface area experienced a decrease as well. The decrease in porosity was more notorious in the ion-exchanged Fe–Al-lie, because approximately 65% of the micropore volume in the fresh sample was not available in the deactivated zeolite.

Studies on benzene hydroxylation with $N_2O$ over iron-containing zeolites have reached equivocal conclusions regarding the deactivation mechanism in terms of coke deposition. Selli et al. [16] stated that deactivation of Fe-MFI was caused by pore blockage due to molecules trapped in their intersections, whereas Ivanov et al. [14,15] concluded that coke poisons the active iron sites, the concentration of which decreased linearly with coke content. The $N_2$ adsorption results presented here do not allow us to exclude any of these possible mechanisms. In fact, their relative contribution to the activity loss appears to be related to the specific catalyst. For example, the limited decrease in micropore volume of Fe–Ga-st after the reaction strongly suggests that the main deactivation mechanism is formation of carbonaceous deposits obstructing the active surface, rather than the total inaccessibility of the active sites within the micropore network due to pore blockage. The coke content in Fe–Ga-st at the end of the experiment was ca. 16% (see Fig. 2). Less coke was formed in Fe–Al-lie (ca. 10%), whereas the microporous properties were more severely affected. Accordingly, pore blockage can be considered more prominent in the ion-exchange catalyst than in the steam-activated catalyst.

### 3.5. Regeneration

Fig. 8 shows selected infrared spectra during air regeneration at 723 K of the zeolites after ODHP at 723 K for 120 min. Previous TEOM studies have shown that the maximum rate of coke burn-off occurs at around 800 K, but longer regeneration periods at 723 K are preferred to run a battery of parallel reactors sequentially at the same temperature during reaction and regeneration [13]. Bands related to the carbonaceous deposits in the C–H stretching region progressively disappear due to coke combustion, and the terminal silanol groups and Brønsted acid centers become distinguishable. Infrared spectra suggest that the 3730 and 3600 $cm^{-1}$ bands in the regenerated samples were not totally restored, implying certain differences with respect to the fresh counterparts. In contrast to this, the porous characteristics of the regenerated and fresh zeolites practically matched (as shown in Table 2 and Fig. 8 for Fe–Ga-st).

A strong indication supporting the change of the catalyst structure in the reaction and regeneration steps stems from the appearance of a band at 3670 $cm^{-1}$ in the regenerated version of the best-performing Fe–Ga-st catalyst, which is not present in the fresh sample (Fig. 8). This new feature is displayed more clearly in Fig. 9, which shows the spectra of the coked and regenerated Fe–Ga-st from two successive runs with the same specimen. The absorption at 3670 $cm^{-1}$ can be assigned to extra-framework gallium cations with Lewis acid character [30] and indicates dislodgement of framework gallium toward extra-lattice positions in the course of the reaction–regeneration cycle. This substantiates that the absorption associated with Brønsted acidity was not fully recovered. Changes in the local environment of gallium on reaction and/or regeneration can certainly affect the iron constitution. Intrapore active iron species are stabilized in ion-exchange positions as isolated and/or oligonuclear species, and the eventual extraction of lattice $Ga^{3+}$ ions connected to such sites will very likely disrupt the structure of the iron center. The spectra of the regenerated sample did not change on successive reaction-regenerated cy-

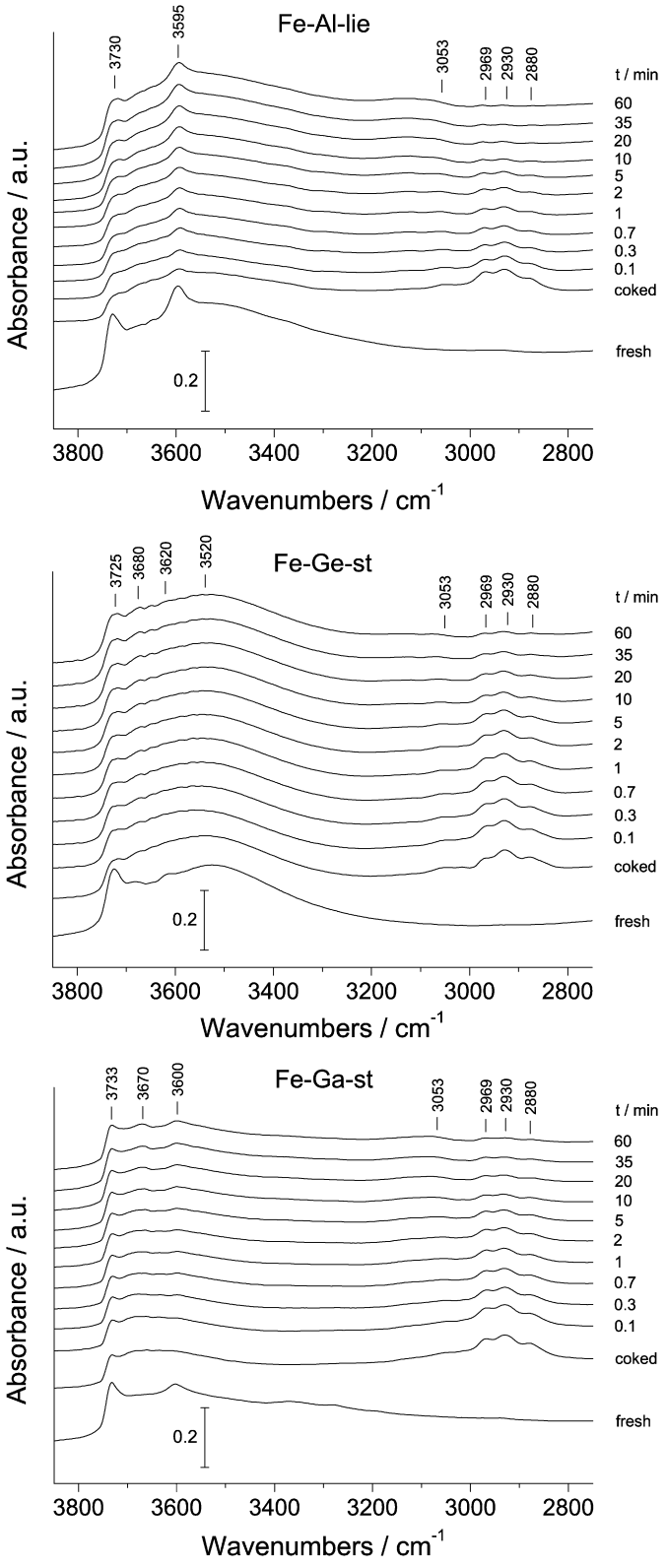


Fig. 8. Infrared spectra of the coked zeolites at selected times during regeneration in air at 723 K. The spectra of the fresh samples are shown for comparative purposes.

cles (see Fig. 9), indicating that the catalyst was stabilized after the first run. As expected, the band at 3670 $cm^{-1}$ disappeared during the second ODHP run, as the formed coke covered the

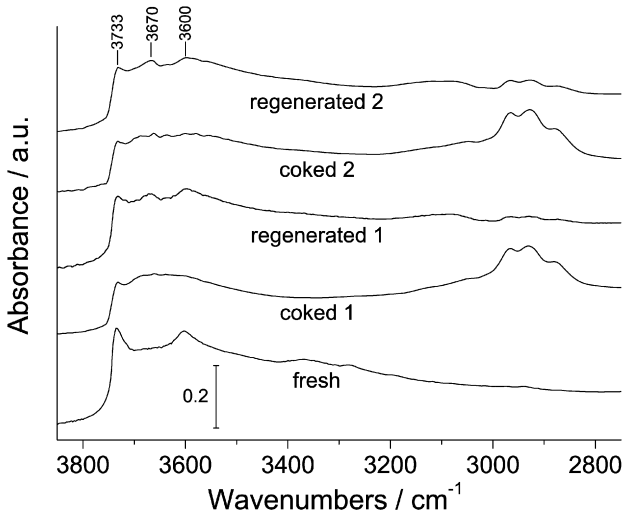


Fig. 9. Infrared spectra of Fe–Ga-st after ODHP reaction (at 723 K for 120 min) and air regeneration (at 723 K for 90 min) in two consecutive runs with the same sample. The spectrum of the fresh zeolite is shown for comparison.

newly generated Lewis sites as well as the remaining Brønsted sites and silanol groups. The new feature in the infrared spectrum of the regenerated Fe–Ga-st catalyst prompted us to compare the ODHP performance of the regenerated and fresh Fe–Ga-st zeolites and to undertake further characterization of the samples.

### 3.6. Fresh versus regenerated catalysts in ODHP

In our previous study over steam-activated Fe–Al-MFI [13], we found that the regenerated zeolite presented practically the same initial and residual propylene yields as the fresh zeolite, but that deactivation of the former sample was significantly faster. A very similar observation was made over Fe–Ga-st using the TEOM–GC analysis (Fig. 10); the initial $C_3H_6$ yield (ca. 22%) was similar in the fresh and regenerated zeolites, but the latter sample suffered faster deactivation. The yield to propylene began to decrease after 20 min on stream, in contrast with the stable performance of the fresh zeolite during the first 80 min on stream. As a result of the higher $C_3H_6$ production, the amount of coke formed determined by the TEOM after 120 min was 4 times higher in the fresh zeolite than in the regenerated zeolite. In agreement, the intensity of the coke-related bands was also lower in the run with the regenerated sample, as shown in Fig. 10 for the infrared absorption at 2930 $cm^{-1}$. However, the ratio of intensities was much lower than the ratio of carbon contents determined by the microbalance. The $Y(C_3H_6)$ versus time profiles in subsequent runs were practically identical to those of the zeolite after the first regeneration, confirming that the catalyst was stabilized after the first reaction–regeneration cycle.

Clearly, the regenerated Fe–Ga-st catalyst did not exhibit the same performance as the fresh zeolite. As shown in the previous section, regeneration in air largely restored the porous properties of the zeolite. Moreover, the crystallinity of the fresh and regenerated samples was identical, as revealed by X-ray diffraction (Fig. 11). We propose that the distinct deactivation

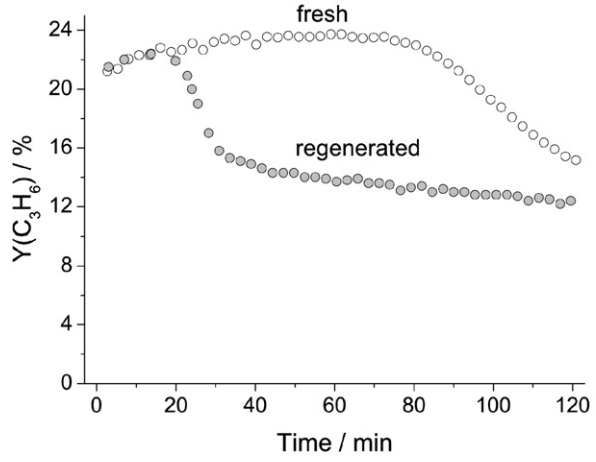


(a)

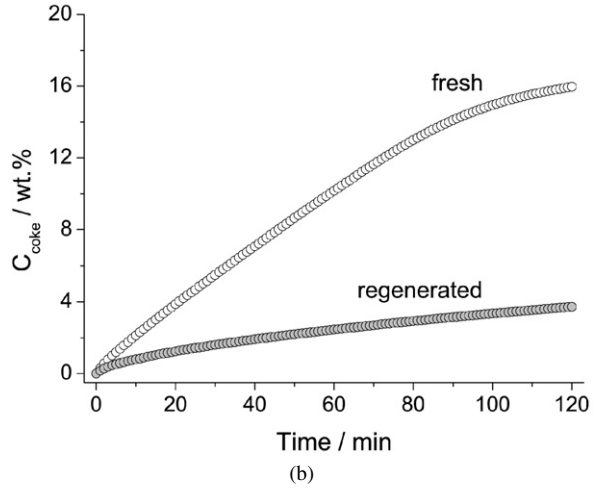


(b)

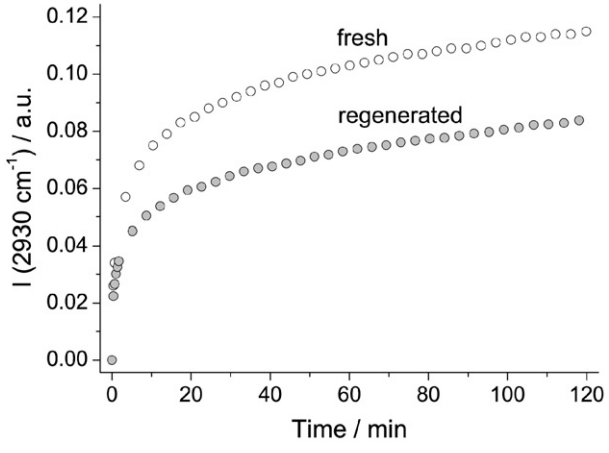


(c)

Fig. 10. (a) Propylene yield, (b) coke content, and (c) intensity of the infrared band at 2930 $cm^{-1}$ during ODHP at 723 K over the fresh and regenerated Fe–Ga-st samples.

behavior can be originated by a change in iron constitution during the first reaction–regeneration cycle. Supporting evidence for this statement comes from the feature at 3670 $cm^{-1}$ in the infrared spectra of the regenerated Fe–Ga-st catalyst, which can be indirectly associated with changes in the local environment of the iron species. This has been supported by TEM studies

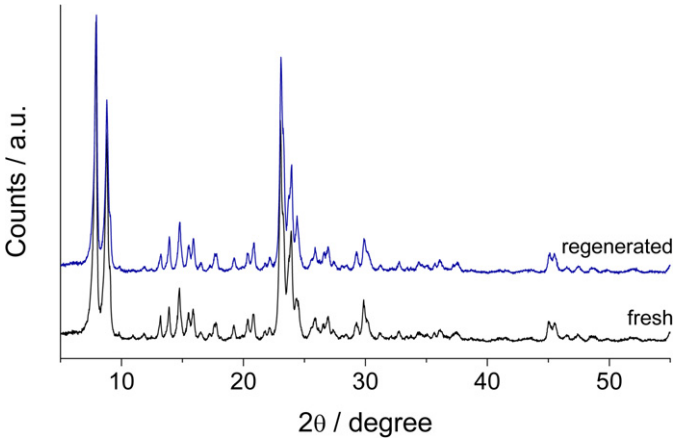


Fig. 11. XRD patterns of the fresh and regenerated Fe–Ga-st samples.

over the zeolites. As shown in Fig. 12, a marked clustering of iron can be seen in the regenerated Fe–Ga-st sample. The iron oxide nanoparticles in the fresh Fe–Ga-st sample were highly dispersed and of uniform size. The histogram given in supplementary material, determined by measuring 100–150 particles in different regions of the specimen using the software package of the microscope, reveals that ca. 95% of the particles were in the narrow range of 1–3 nm. The oxidic nanoparticles in the regenerated specimen were significantly larger and have a broader size distribution (3–7 nm, centered at 5 nm). Occasionally, larger particles were also identified (up to 30 nm; see the bottom-right micrograph in Fig. 12). The latter observation was not made in any of the multiple spots scouted over the fresh zeolite. Despite the marked degree of clustering in the regenerated sample, no reflections associated with $Fe_2O_3$ were revealed by XRD (Fig. 11). This is likely due to the relatively low amount of this oxidic phase (the total iron content in the sample was 0.6 wt%) and/or its amorphous nature. TEM investigations also made it possible to conclude that the size and distribution of $FeO_x$ entities in the coked sample resemble those in the fresh zeolite (Fig. 12), strongly suggesting that alteration of the catalyst structure leading to clustering of iron species occurs mainly during coke burn-off.

Our results demonstrate for the first time that the regeneration of iron-containing zeolites in $N_2O$-mediated selective oxidations is not fully reversible. In situ infrared spectroscopy in combination with TEOM–GC and additional characterization enabled us to monitor the processes and explain this behavior. The absorption band at 3670 $cm^{-1}$ assigned to the extraction of framework gallium entails a change in the nature of the associated extra-framework iron species, resulting in extensive clustering as confirmed by TEM. It is widely established that the active extra-framework iron species in selective oxidation over Fe-zeolites are located in the micropore system and are stabilized in ion-exchanged positions as isolated and oligonuclear iron species, whereas iron oxide nanoparticles at the external surface are inactive [2]. The fact that the initial propylene yields over the fresh and regenerated zeolites were practically coincident suggests that the most effective iron species for ODHP retained their structure after the first reaction–regeneration cycle. However, alteration of the iron constitution resulted in a

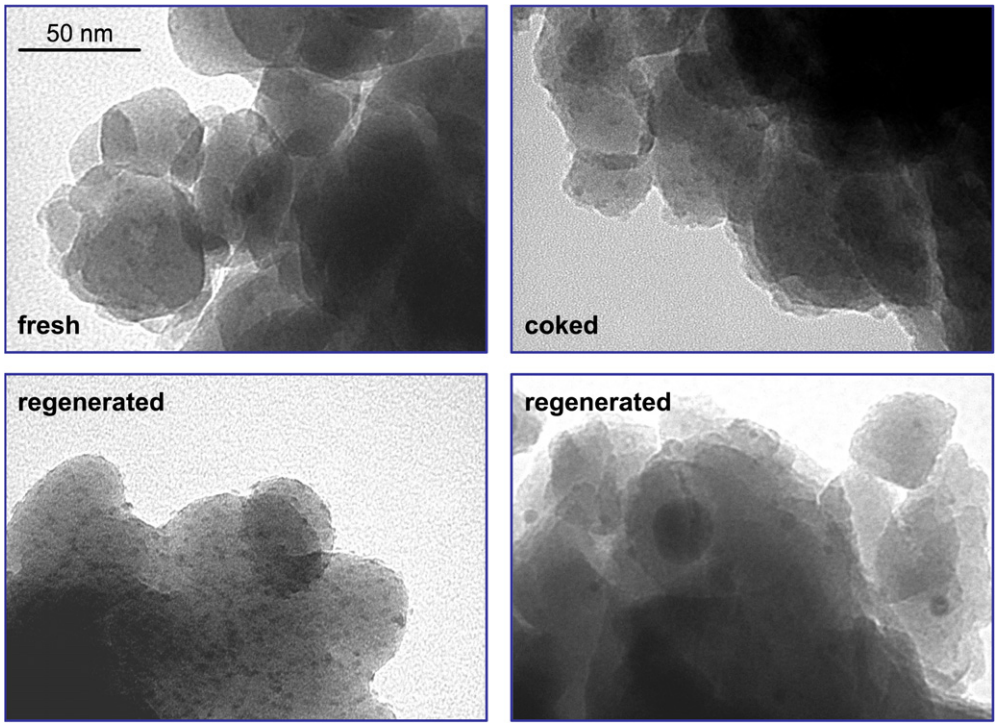


Fig. 12. TEM images of fresh, coked, and regenerated Fe–Ga-st. The scale bar (top, left) applies to all the micrographs.

catalyst with lower resistance to coke deactivation and/or a reduced number of active sites by clustering. Accordingly, the regenerated zeolite was able to maintain high levels of propylene production for a considerably shorter period compared with the fresh counterpart. Appropriate strategies for catalyst regeneration should be designed to avoid modification of the iron speciation on coke removal leading to diminished ODHP performance. We put forward that the conclusions derived from this study apply to other actual or prospective applications of $N_2O$ as selective oxidant of hydrocarbons over Fe-zeolites, because deactivation by coke and generation are common denominators.

## 4. Conclusion

In situ infrared spectroscopy has provided valuable insights into the deactivation of iron-containing zeolites in ODHP with $N_2O$ and their subsequent regeneration in air. DRIFTS proved rather complementary to TEOM–GC experiments, stressing the importance of integrating in situ techniques to monitor deactivation and derive a solid understanding of catalytic processes. Coke formation, connected to the presence of strong acidic protons in the zeolite and trivalent cations ($Fe^{3+}$, $Ga^{3+}$, and $Al^{3+}$) as electron acceptor sites, was very fast. The nature of coke was similar in the different samples, despite their markedly different catalytic performance. Deactivation of Fe-zeolites in ODHP was caused mainly by coke deposition in active extra-framework iron species. Coke deposits can be removed by air treatment, largely restoring the porous properties of the original zeolite and having no effect on the crystallinity. The regeneration process is not completely reversible, however; the initial propylene yield was equal in the fresh and regenerated samples, but the latter exhibited faster deactivation. This finding can be explained by the alteration of iron speciation in the catalyst during the first reaction–regeneration cycle. In particular, it was proven that air treatment of the spent sample for coke burn-off caused significant iron clustering, leading to a reduced number of active sites and thus a less efficient catalyst for ODHP. Regeneration strategies should be carefully designed to avoid iron site modification.

## Acknowledgments

This research was supported by the Spanish MEC (project CTQ2006-01562/PPQ and Consolider-Ingenio 2010 grant CSD2006-003) and the ICIQ Foundation.

## Supplementary material

The online version of this article contains additional supplementary material.

Please visit DOI: 10.1016/j.jcat.2007.04.010.

## References

[1] G.I. Panov, A.K. Uriarte, M.A. Rodkin, V.I. Sobolev, Catal. Today 41 (1998) 365.
[2] G.I. Panov, CATTECH 4 (2000) 18.
[3] K. Nowińska, A. Wącław, A. Izbińska, Appl. Catal. A 243 (2003) 225.
[4] J. Pérez-Ramírez, E.V. Kondratenko, Chem. Commun. (2003) 2152.
[5] R. Bulánek, B. Wichterlová, K. Novoveská, V. Kreibich, Appl. Catal. A 264 (2004) 13.
[6] E.V. Kondratenko, J. Pérez-Ramírez, Appl. Catal. A 267 (2004) 181.
[7] A.H. Tullo, Chem. Eng. News 81 (2003) 15.
[8] J. Pérez-Ramírez, A. Gallardo-Llamas, Appl. Catal. A 279 (2005) 117.
[9] O.V. Buyevskaya, M. Baerns, Catalysis 16 (2002) 155.

[10] J. Pérez-Ramírez, A. Gallardo-Llamas, J. Catal. 223 (2004) 382.
[11] J. Pérez-Ramírez, A. Gallardo-Llamas, J. Phys. Chem. B 109 (2005) 20529.
[12] J. Pérez-Ramírez, A. Gallardo-Llamas, C. Daniel, C. Mirodatos, Chem. Eng. Sci. 59 (2004) 5535.
[13] A. Gallardo-Llamas, C. Mirodatos, J. Pérez-Ramírez, Ind. Eng. Chem. Res. 44 (2005) 455.
[14] D.P. Ivanov, M.A. Rodkin, K.A. Dubkov, A.S. Kharitonov, G.I. Panov, Kinet. Catal. 6 (2000) 771.
[15] D.P. Ivanov, V.I. Sobolev, G.I. Panov, Appl. Catal. A 241 (2003) 113.
[16] E. Selli, I. Rossetti, D. Meloni, F. Sini, L. Forni, Appl. Catal. A 262 (2004) 131.
[17] R. Josl, R. Klingmann, Y. Traa, R. Gläser, J. Weitkamp, Catal. Commun. 5 (2004) 239.
[18] A. Satsuma, A.D. Cowan, N.W. Cant, D.L. Trimm, J. Catal. 181 (1999) 165.
[19] H.G. Karge, W. Nießen, H. Bludau, Appl. Catal. 146 (1996) 339.
[20] J. Saussey, F. Thibault-Starzyk, in: B.M. Weckhuysen (Ed.), In Situ Spectroscopy of Catalysts, American Scientific Publishers, Stevenson Ranch, 2004, pp. 15–31.
[21] P. Kubánek, B. Wichterlová, Z. Sobalík, J. Catal. 211 (2002) 109.
[22] B. Wichterlová, Z. Tvarůžková, Z. Sobalík, P. Sarv, Microporous Mesoporous Mater. 24 (1998) 223.
[23] J. Pérez-Ramírez, F. Kapteijn, J.C. Groen, A. Doménech, G. Mul, J.A. Moulijn, J. Catal. 214 (2003) 33.
[24] J. Pérez-Ramírez, J. Catal. 227 (2004) 512.
[25] S. Brunauer, P.H. Emmet, E. Teller, J. Am. Chem. Soc. 60 (1938) 309.
[26] B.C. Lippens, J.H. de Boer, J. Catal. 4 (1965) 319.
[27] S. Bordiga, R. Buzzoni, F. Geobaldo, C. Lamberti, E. Giamello, A. Zecchina, G. Leofanti, G. Petrini, G. Tozzola, G. Vlaic, J. Catal. 158 (1996) 486.
[28] A. Jentys, J.A. Lercher, in: H. van Bekkum, P.A. Jacobs, J.C. Jansen (Eds.), Introduction to Zeolite Science and Practice, Elsevier, Amsterdam, 2001, p. 345.
[29] M. Trombetta, G. Busca, S. Rossini, V. Piccoli, U. Cornaro, J. Catal. 168 (1997) 349.
[30] L. Čapek, K. Novoveská, Z. Sobalík, B. Wichterlová, L. Cider, E. Jonson, Appl. Catal. B 60 (2005) 201.
[31] L.G.A. van der Water, J.C. van der Waal, J.C. Jansen, M. Cadoni, L. Marchese, T. Maschmeyer, J. Phys. Chem. B 107 (2003) 10423.
[32] H. Kosslick, V.A. Tuan, R. Fricke, Ch. Peuker, W. Pilz, W. Storek, J. Phys. Chem. 97 (1993) 5678.
[33] A. Zecchina, F. Geobaldo, C. Lamberti, S. Bordiga, G. Turnes Palomino, C. Otero Aréan, Catal. Lett. 42 (1996) 25.
[34] J. Pérez-Ramírez, M.S. Kumar, A. Brückner, J. Catal. 223 (2004) 13.
[35] G. Yaluris, J.E. Rekosket, L.M. Aparicio, R.J. Madon, J.A. Dumesic, J. Catal. 153 (1995) 54.
[36] M. Boronat, P.M. Viruela, A. Corma, J. Am. Chem. Soc. 126 (2004) 3300.
[37] P. Andy, N.S. Gnep, M. Guisnet, E. Benazzi, C. Travers, J. Catal. 173 (1998) 322.
[38] K.S.W. Sing, D.H. Everett, R.A.W. Haul, L. Moscou, R.A. Pierotti, J. Rouquerol, T. Siemieniewska, Pure Appl. Chem. 57 (1985) 603.